LIMNOLOGY and OCEANOGRAPHY

ASLO

Limnol. Oceanogr. 70, 2025, 2125–2141
© 2025 Association for the Sciences of Limnology and Oceanography.
doi: 10.1002/lno.70105

RESEARCH ARTICLE

Unexpectedly stable soil organic carbon in tidal marshes under combined nitrogen loading and increased inundation compared to individual effects

Tianning Fan,[1] Jiafang Huang,[2,3] Guopeng Liang,[4,5] Shengen Liu,[6] Dehong Hu,[1] Lifei Su,[1] Yi Liu,[1] YuanBin Cai,[1] Shihua Li,[7] Pingping Guo,[8] Min Luo ,[1*] Chuan Tong [2,3*]

[1]College of Environment and Safety Engineering, Fuzhou University, Fuzhou, China; [2]Institute of Geography, Fujian Normal University, Fuzhou, China; [3]Key Laboratory of Humid Subtropical Eco-Geographical Process, Ministry of Education, Fujian Normal University, Fuzhou, China; [4]Department of Ecology and Evolutionary Biology, Yale University, New Haven, Connecticut, USA; [5]Institute for Global Change Biology and School for Environment and Sustainability, University of Michigan, Ann Arbor, Michigan, USA; [6]College of Forestry, Fujian Agriculture and Forestry University, Fuzhou, China; [7]College of Advanced Manufacturing, Fuzhou University, Jinjiang, China; [8]Fujian Minjiang River Estuary Wetland National Nature Reserve Administrative Office, Fuzhou, China

Abstract

Tidal marshes serve as critical carbon (C) sinks, yet face increasing threats from global environmental changes. While previous research has documented how nitrogen (N) loading and sea-level rise affect total C pools individually, their impacts on soil organic carbon (SOC) stabilization remain critically underexplored, particularly when these factors co-occur in tidal marsh ecosystems. Through a 3-yr field experiment, we analyzed how these factors, alone and combined, impact SOC stabilization by examining SOC fraction dynamics. Results showed that N loading increased particulate organic carbon (POC) by 18% and decreased mineral-associated organic carbon (MAOC) by 13%, reducing SOC stabilization. Conversely, increased inundation raised MAOC by 31% and decreased POC by 19%, promoting SOC stabilization. The decreased MAOC under N loading stemmed from reduced fungal necromass C, while the increased POC related to lower phenol oxidase activity. In contrast, with increased inundation, MAOC rose due to iron-bound organic C (Fe-OC) accumulation, while POC declined from increased phenol oxidase activity. When both factors were applied together, SOC stabilization remained at control levels. This occurred because the combined effect maintained oxidative enzyme activities and thus retained POC levels. The simultaneous reduction in fungal necromass C and enhancement of Fe-OC associations established complementary mechanisms that maintained MAOC at levels equivalent to control. Our findings reveal that N loading and increased inundation drive contrasting patterns of SOC stabilization, while their combination produces uniquely stabilized C dynamics. This insight challenges single-factor predictions and underscores the importance of multi-factor experiments in understanding ecosystem responses under concurrent global change scenarios.

Tidal marshes, influenced by marine tides and characterized by halophytic vegetation on freshwater to saline mudflats, rank among the most productive ecosystems globally (Wang et al. 2021a; Macreadie et al. 2021). With carbon burial rates reaching 218 g m^{-2} yr^{-1}—approximately 40 times higher than forest ecosystems—these environments serve as exceptional carbon (C) sinks (Duarte et al. 2013; Macreadie et al. 2019; Sapkota and White 2021). Consequently, even minor fluctuations in soil organic carbon (SOC) pools within tidal marshes could substantially impact atmospheric CO_2 concentrations (Campbell et al. 2022). As natural climate solutions, tidal marshes offer significant potential for climate change mitigation through conservation and restoration efforts worldwide

*Correspondence: luomin@fzu.edu.cn; tongch@fjnu.edu.cn

Associate editor: Perran Cook

Data Availability Statement: Data deposited in the Figshare, http://doi.org/10.6084/m9.figshare.29105297. We used no unreported custom computer code or algorithm.

(Taillardat et al. 2020). However, impending global changes, particularly nitrogen (N) loading and sea-level rise, threaten to fundamentally alter these critical carbon reservoirs (Han et al. 2021). N loading has increased dramatically in coastal areas, with oceanic discharges expanding at least tenfold since pre-industrial times (Breitburg et al. 2018). Concurrently, global sea levels have risen 16–21 cm since 1900 and continue to increase approximately 3.5 mm annually (Bagnell and DeVries 2023), intensifying inundation events in tidal marshes (Luo et al. 2019; Sandi et al. 2021). Notably, these environmental stressors frequently occur simultaneously in industrialized and densely populated coastal regions, which experience both accelerated N loading and increased inundation from rising sea levels (Sapkota and White 2021; Tong et al. 2024). While numerous studies have examined how total C pool respond to each of these global changes individually, SOC stabilization dynamics under multiple simultaneous stressors remain largely unexplored, particularly regarding potential interactive effects when both factors operate concurrently.

Soil organic carbon stabilization refers to the soil's capacity to efficiently retain SOC over extended periods (Lehmann et al. 2020). Even soils currently exhibiting high SOC contents may not maintain these levels under future global changes (Macreadie et al. 2021; Cotrufo and Lavallee 2022). Consequently, investigating SOC stabilization under projected climate scenarios provides greater insights than merely studying SOC contents (Tang et al. 2023). While directly measuring SOC stabilization remains challenging, analyzing different SOC fractions offers an effective approach for understanding SOC stabilization mechanisms and predicting future outcomes (Lavallee et al. 2020). Soil organic carbon can be physically separated into particulate organic carbon (POC, $> 53\ \mu$m) and mineral-associated organic carbon (MAOC, $< 53\ \mu$m). Particulate organic carbon primarily consists of aboveground plant residues and root tissues (Angst et al. 2021) and remains vulnerable to enzymatic breakdown and microbial decomposition (Whalen et al. 2022). In contrast, MAOC forms when small organic molecules—either leached from plants or modified through microbial processes—become stabilized through chemical bonding with soil minerals (Cotrufo and Lavallee 2022). For instance, iron-bound organic carbon (Fe-OC), a critical component of MAOC, develops through interactions between organic carbon and iron oxide [Fe(III)] minerals (Hu et al. 2023). With turnover times spanning decades to centuries, MAOC contributes substantially to long-term carbon sequestration (Lavallee et al. 2020). The MAOC/POC ratio thus serves as a valuable indicator of SOC stabilization potential, where higher ratios suggest enhanced carbon preservation capacity (Sokol and Bradford 2019; Lavallee et al. 2020).

Nitrogen loading and sea-level rise may influence SOC stabilization through several complex and potentially contradictory mechanisms. While N loading typically enhances aboveground plant biomass and plant-derived C inputs, potentially promoting POC formation (Huang and Hall 2017; Liang et al. 2021), it can simultaneously accelerate the decomposition of plant litter with high C/N ratios, potentially reducing POC accumulation (Knorr et al. 2024). For MAOC dynamics, enhanced N availability stimulates microbial processes that transform plant-derived C into residues and metabolites readily associating with mineral surfaces, enhancing MAOC formation (Liang et al. 2019; Cotrufo et al. 2019); yet contradictorily, N loading may decrease fungal dominance due to increased nutrient availability, reducing soil fungal necromass—a key contributor to MAOC (Widdig et al. 2020; Sun et al. 2023). Similarly, increased inundation presents its own set of opposing mechanisms: it typically reduces plant biomass production, potentially decreasing POC formation (Sandi et al. 2021), while simultaneously promoting anaerobic conditions and suppressing oxidative C-acquiring enzyme activities, which may conversely preserve POC (Freeman et al. 2001; Lavallee et al. 2020). For MAOC dynamics under inundation, anaerobic conditions may hinder formation by affecting sorption and co-precipitation of organic C compounds onto mineral surfaces (Hagh-Doust et al. 2023; Hu et al. 2023), while wetland plants often respond to inundation by enhancing oxygen transport through root aerenchyma (Armstrong et al. 2000; Liu et al. 2021), potentially oxidizing the rhizosphere and stimulating Fe(III) precipitation that binds organic C, thereby enhancing MAOC formation (Hu et al. 2023; Tan et al. 2025). Given these complex and often contradictory mechanisms, the combined effects of N loading and increased inundation may produce unexpected interactions rather than simply additive outcomes, highlighting the necessity of multifactor field experiments to elucidate the direction, magnitude, and mechanisms of carbon-climate feedback in tidal marsh ecosystems under realistic global change scenarios.

To bridge this knowledge gap, here we investigated changes in SOC stabilization, represented by the ratios of MAOC to POC, in response to N loading and increased inundation in a tidal marsh ecosystem. To achieve this, we established four in-situ treatments: control, N loading (N), increased inundation (I), and the combination of N loading and increased inundation (N + I), monitored over a 3-yr period. We hypothesized that: (i) N loading would decrease SOC stabilization by increasing POC through enhanced plant biomass production and reducing MAOC via a shift in microbial community composition towards a lower fungal/bacterial ratio; (ii) increased inundation would similarly reduce SOC stabilization by promoting POC accumulation through the suppression of C-acquiring enzyme activities under anaerobic conditions, while also diminishing MAOC due to reduced soil Fe(III) concentrations; and (iii) the combined effects of N loading and increased inundation would produce interactive effects on SOC stabilization that could differ from predictions based solely on their individual effects. This study presents the first

experimental evidence of interactive effects between N loading and increased inundation on SOC stabilization in tidal marshes, revealing mechanisms that challenge predictions based on single-factor experiments and providing insights into how these ecosystems respond to concurrent global changes. Understanding these interactive effects is critical for accurate C accounting in blue carbon ecosystems and can inform evidence-based coastal management strategies under multiple global change drivers.

Materials and methods

Experiment design

The study site is located in the tidal marsh of Shanyutan in the Min River Estuary, southeast China (119°34′12″–119°40′40″ E, 26°00′36″–26°03′42″ N). This region is characterized by a mean annual precipitation of 1200 to 1740 mm and an average air temperature ranging from 19.8 to 21.3°C (Luo et al. 2020). Dominated by the native tidal marsh species *Cyperus malaccensis* Lam., the study site is subjected to regular semi-diurnal tides with an inundation period of approximately 5–8 h per day. Tidal water typically has a salinity of 4.2 ± 2.5 psu (practical salinity units; Chen et al. 2022).

Four treatments were established at the study site: control, N loading (N), increased inundation (I), and a combination of N loading and increased inundation (N + I) (Fig. 1). Twelve square experimental weirs (each 1 m^2) were randomly assigned to the four treatments, with each treatment having three replicates. Each weir was constructed from four polypropylene walls, each with a height of 100 cm, and buried 35 cm into the ground. The weirs were spaced 3 m apart to minimize cross-contamination. After 2 weeks of operation, one experimental plot was damaged, so we established a replacement plot outside the boardwalk to maintain the experimental design integrity. All experimental plots remained subject to local tidal cycles throughout the study period.

For the inundation treatments (I and N + I), weirs were equipped with two holes (5 cm diameter) drilled into their sides at ground level facing the sea (Supporting Information Fig. S1). The first hole contained a one-way check valve allowing passive entry of tidal water while restricting outflow, while the second featured a 30 cm PVC pipe fitted with a floating ball valve that regulated drainage during ebb tides (Cherry et al. 2015). This design extended inundation duration by approximately 6 h and increased water height by 6.5 cm compared to non-inundation treatments (Supporting Information Fig. S1), simulating approximately 20 yr of future sea-level rise based on the local rate of 3.2 mm yr^{-1} (Hu et al. 2023). In contrast, control and N loading treatment weirs contained a single unobstructed hole that maintained natural tidal flow patterns without prolonged inundation.

For N loading treatments (N and N + I), we applied a mixed solution of $NaNO_3$ and NH_4Cl (2 : 1 ratio) dissolved in 2 L of tidal creek water, reflecting the proportions of N forms typically found at the study site (Tong et al. 2024). Solutions were applied biweekly following neap tide ebb to maximize soil

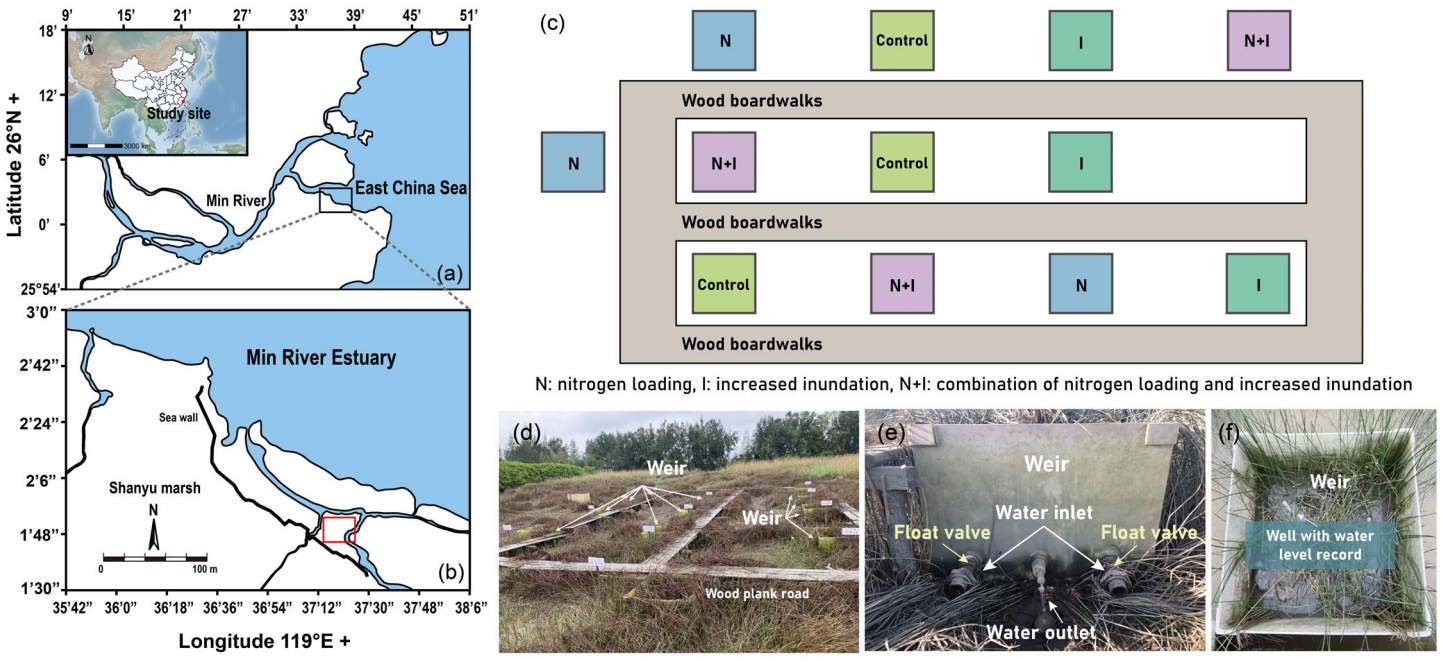


Fig. 1. Experiment design. Location of the study area (**a**, **b**). Layout of the four experimental treatments: control, nitrogen loading (N), increased inundation (I), and the combination of nitrogen loading and increased inundation (N + I) (**c**). Photos of the experimental site (**d**), side (**e**), and plan (**f**) views of weir.

retention, followed by an additional 2 L of tidal water to wash any remaining solution from plant surfaces onto the soil. The annual N application rate (48 g N m^{-2} yr^{-1}) was approximately double the current total N loading in the Min River Estuary from atmospheric deposition, runoff, and tidal exchange (Yu et al. 2019), representing a moderate eutrophication scenario projected for similar coastal systems. To maintain consistent moisture conditions across all treatments, non-N loading treatments (control and I) received 4 L of tidal water on the same application schedule.

Sample collection

The experiment was initiated in November 2018 and concluded in August 2021, spanning 3 yr. Samples of plants and soils were collected during three distinct sampling events: July 2019 (after 240 d), August 2020 (after 630 d), and August 2021 (after 1000 d). Consistent seasonal sampling across years minimizes the effects of seasonal variation on our measured parameters. We chose summer sampling because summer represented the peak growing season when plant productivity and microbial activity are maximized, providing optimal conditions to observe treatment effects on soil C dynamics. During sampling, three soil cores measuring 10 cm in depth were extracted from each weir using a steel soil sampler, as this surface layer is most directly affected by both N deposition and inundation treatments, allowing us to capture the most pronounced treatment effects. The soil subsamples for edaphic condition analysis and anaerobic incubation were stored at 4°C, while those for measuring microbial properties were frozen at −20°C.

Edaphic conditions

The soil moisture content and bulk density were determined by oven-drying the samples at 105°C until they reached a constant weight. The concentrations of NH_4^+ and NO_3^- were measured using a flow injection analyzer (SAN++; Skalar Analytical, Breda, Netherlands). The salinity was measured by a SALT 6 + salinity meter (Thermo Fisher Scientific, Waltham, MA, USA) with a detection accuracy of 0.1 psu. The concentration of SO_4^{2-} in the porewater was measured by ion chromatography (Dionex 2100; Thermo Fisher Scientific, Waltham, MA, USA). The soil pH was measured in situ with a pH meter (No. pH 400; Spectrum Technologies Inc., Paxinos, PA, USA). The concentration of dissolved organic carbon (DOC) was measured with a total organic C analyzer (TOC-V CPH; Shimadzu Corp., Kyoto, Japan). The SOC and total nitrogen (TN) contents were also measured with a Vario MAX CN elemental analyzer (Elementar Analysensysteme GmbH, Hesse, Germany). Soil Fe(II) and total Fe contents were detected by photometric analyses using a spectrophotometer (Shimadzu UV-2450, Tokyo, Japan) (Kostka and Luther 1994). Soil Fe(III) content was calculated by subtracting the Fe(II) content from the total Fe. We used soil Fe(III):Fe(II) ratios as a proxy for the potential of redox condition in this study (Liu et al. 2021).

Plant biomass and microbial properties

Plant samples were collected for biomass determination. The aboveground and belowground portions were individually covered with nylon mesh bags (1 mm pore size) and washed, and then dried at 65°C to determine their biomass.

The bacterial and fungal biomasses were assessed by phospholipid fatty acid analysis (PLFA) using a gas chromatograph (6890, Agilent, USA; Frostegård et al. 2011). The fatty acids were analyzed to identify individual PLFAs. Each fatty acid was measured by comparing each fatty acid's individual peak area to the internal standard C19:0. Based on their origins, several microbial groupings were assigned to PLFA biomarkers. Different PLFA biomarkers were assigned to specific functional microbial groups according to Fan et al. (2023).

Fluorometric analysis was used to quantify the activities of β-1,4-glucosidase (BG), whereas colorimetric microplate assays were used to measure the activities of phenol oxidase (POX) (Saiya-Cork et al. 2002). The activities of soil extracellular enzymes were measured using a microplate reader (Hybrid Technology, USA).

The microbial necromass C (MNC) content was determined based on the amounts of amino sugars (Liang et al. 2019). Amino sugars, including glucosamine (GluN), galactosamine (GalN), and muramic acid (MurN), were quantified using a gas chromatograph (GC 2010 Plus, Shimadzu, Japan). The relative preservation of fungal and bacterial necromass C (FNC and BNC) was assessed using the glucosamine to muramic acid ratio. This calculation assumed a 1 : 2 M ratio of GluN to MurA in bacterial cells. The detailed calculations are provided using Eqs. 1 and 2 (Liang et al. 2019):

$$\text{Fungal necromass} = \left(\frac{\text{GluN}}{179.17} - 2 \times \frac{\text{MurA}}{251.23}\right) \times 179.17 \times 9 \quad (1)$$

$$\text{Bacterial necromass} = \text{MurA} \times 45 \quad (2)$$

where 179.17 and 251.23 denote the molecular weights of GluN and MurA, respectively, while 9 and 45 are the conversion factors for GluN to fungal necromass C and MurA to bacterial necromass C (Appuhn et al. 2006).

Soil organic carbon fractions and stabilization

Using a wet sieving process, SOC was divided into POC and MAOC (Cotrufo et al. 2019). In short, 50 mL of a 5% sodium hexametaphosphate solution was poured into a 50 mL polycarbonate centrifuge tube containing 5 g of air-dried soil (< 2 mm). Samples underwent 1 h of shaking at 180 rpm. After the soil was dispersed, it was rinsed and placed on a 53-μm sieve. The fraction that passed through the sieve (< 53 μm) was collected as MAOC, while the portion that stayed on the sieve (53–2000 μm) was collected as POC. Each fraction was oven-dried at 60°C and its C concentration was measured. Soil organic carbon stabilization was characterized by the ratios of MAOC to POC (Lugato et al. 2021).

The Fe-OC was quantified by the citrate-bicarbonate-dithionite (CBD) method (Lalonde et al. 2012). Each soil sample was split into two subsamples. One subsample was extracted using 1.85 mol L^{-1} sodium chloride and 0.11 mol L^{-1} sodium bicarbonate as the control group. The other subsample was extracted using 0.27 mol L^{-1} trisodium citrate, 0.11 mol L^{-1} sodium bicarbonate, and 0.1 mol L^{-1} sodium dithionite as the treatment group (Patzner et al. 2020). The SOC in these subsamples was then determined using the Vario EL III elemental analyzer (Elementar, Hanau, Germany). The difference in C content between the control and treatment groups represents Fe-OC content.

Statistical analyses

The R program (version 4.1.3) was used to analyze the data. The data were log-transformed before analysis if they did not pass the Shapiro–Wilk normality test. The effects of N loading and increased inundation on edaphic conditions, plant biomass and microbial properties, as well as SOC fractions and stabilization were analyzed using a linear mixed-effect model (LME) performed with the "*nlme*" R function (Pinheiro et al. 2011). In these analyses, treatments and sampling times were treated as fixed factors, and the plots were hierarchically arranged as random factors. When the LME's results showed significant differences, a least-significant-difference (LSD) test was conducted to elucidate multiple comparisons. The correlations between variables were assessed using regression analysis with the "*lm*" function in R, with statistical significance set at $p < 0.05$.

Random Forest analysis was used to ascertain the main drivers controlling SOC fractions with the "*randomForest*" function in "*rfPermute*" R packages (Liaw and Wiener 2002; Archer 2016). Furthermore, we evaluated the models' significance and used the "*A3*" R package to cross-validate r^2 using 5000 possible combinations of the response variables (Fortmann-Roe 2013).

Structural equation modeling (SEM) was utilized to gain a mechanistic understanding of how N loading and increased inundation affect SOC stabilization using the "*piecewiseSEM*" R package (Lefcheck 2016). Shipley's d-separation test was used to evaluate the goodness-of-fit of the SEM with Fisher's C statistic and Akaike's information criterion (AIC) for small sample size as an additional guide (Rosseel 2012; Shipley 2013).

Results

Treatment effectiveness assessments

Our results showed that N loading significantly increased concentrations of NO_3^-, NH_4^+, TN while decreasing C/N ratios (Table 1), confirming the effectiveness of our N loading treatment. However, increased inundation did not significantly alter soil bulk density, moisture content, salinity, pH, or sulfate concentrations (Table 1). The absence of differences in soil bulk density and moisture content between treatments did not suggest experimental failure. Our study site experienced regular tidal flooding (twice daily), and the tidal marsh soils contain high clay content that efficiently retain water even during low tide periods, with soils maintaining consistently high moisture levels under natural conditions. Although soil moisture measurements did not reveal significant differences, the extended daily submergence time was perceived by plants, triggering higher root oxygen loss, as indicated by higher soil Fe(III) and Fe(III)/Fe(II) ratios (Table 1). The lack of difference in salinity, pH, or sulfate concentrations between treatments indicated our inundation treatment did not involve changes in salinity (Table 1).

Changes in soil organic carbon fractions, pool, and stabilization

Across four treatments, POC ranged from 4.2 to 8.4 g kg^{-1} (Fig. 2a), whereas MAOC and Fe-OC ranged from 7.6 to 15.3 g kg^{-1} and from 2.5 to 8.3 g kg^{-1}, respectively (Fig. 2b,c). Particulate organic carbon constituted 22–42% of SOC (Fig. 2d), while MAOC and Fe-OC contributed 37–73% and 13–39% of SOC, respectively (Fig. 2e,f). N loading significantly increased POC by 18% but reduced MAOC by 13% (Fig. 2a,b). In contrast, increased inundation led to a 19% reduction in POC, while enhancing MAOC and Fe-OC by 31% and 69%, respectively (Fig. 2a–c). The combined effect of N loading and increased inundation did not result in significant changes to POC and MAOC (Fig. 2a,b). However, the combined effect increased Fe-OC (Fig. 2c).

Neither treatment, sampling time, nor their combination affected total SOC pool (Fig. 3a). However, SOC stabilization varied across treatments (Fig. 3b). Specifically, N loading decreased both SOC stabilization, while increased inundation enhanced it (Fig. 3b). The combination of N loading and increased inundation, however, did not significantly impact SOC stabilization (Fig. 3b). The total SOC pool was unrelated to SOC stabilization (Fig. 3c).

Environmental drivers of soil organic carbon fractions

Nitrogen loading did not change either aboveground or belowground biomass (Table 2). Increased inundation did not alter aboveground biomass but increased belowground biomass (Table 2). N loading reduced fungal/bacterial ratios, phenol oxidase activity, and fungal necromass C, while increased inundation elevated activities of both phenol oxidase and β-1,4-glucosidase (Table 2). Increased inundation did not significantly affect fungal necromass C; however, the combined effect of increased inundation and N loading decreased fungal necromass C (Table 2).

We conducted the Random Forest modeling to screen the potential edaphic, plant, and microbial drivers of POC, MAOC, and Fe-OC (Fig. 4a–c). For POC, microbial drivers dominated (51%), followed by edaphic drivers (37%) and plant drivers (12%). Mineral-associated organic carbon showed a more balanced distribution between edaphic drivers (42%)

Table 1. Effects of nitrogen loading (N), increased inundation (I), and the combination of nitrogen loading and increased inundation (N + I) on edaphic conditions at 240 d, 630 d, and 1000 d ($n = 3$). N: nitrogen loading; I: increased inundation; N + I: combination of nitrogen loading and increased inundation.

		Treatments					
Variables	**Time (d)**	**Control**	**N**	**I**	**N + I**		***p***
Bulk density (g cm^{-3})	240	1.2 ± 0.1	1.1 ± 0.0	1.1 ± 0.0	1.2 ± 0.0	Treatment	*n.s.*
	630	1.2 ± 0.1	1.2 ± 0.1	1.2 ± 0.1	1.2 ± 0.1	Time	*n.s.*
	1000	1.2 ± 0.1	1.3 ± 0.0	1.2 ± 0.1	1.2 ± 0.0	Interaction	*n.s.*
	Average	1.2 ± 0.1A	1.2 ± 0.1A	1.2 ± 0.1A	1.2 ± 0.1A		
Moisture content (%)	240	47.7 ± 3.3	50.2 ± 3.4	47.6 ± 4.0	48.5 ± 4.2	Treatment	*n.s.*
	630	46.3 ± 4.5	45.8 ± 3.1	48.8 ± 2.6	48.2 ± 2.3	Time	*n.s.*
	1000	48.1 ± 6.6	49.2 ± 2.3	47.2 ± 5.2	45.5 ± 9.1	Interaction	*n.s.*
	Average	47.4 ± 4.4A	48.4 ± 3.3A	47.9 ± 3.6A	47.4 ± 5.3A		
Salinity (practical salinity units)	240	3.1 ± 0.4	3.2 ± 0.3	2.7 ± 0.4	2.9 ± 0.6	Treatment	*n.s.*
	630	2.6 ± 0.3	2.3 ± 0.4	2.2 ± 0.2	2.5 ± 0.3	Time	*
	1000	3.1 ± 0.4	2.8 ± 0.1	1.9 ± 0.8	2.6 ± 0.7	Interaction	*n.s.*
	Average	2.9 ± 0.4A	2.8 ± 0.4A	2.3 ± 0.6A	2.7 ± 0.5A		
SO_4^{2-} (mmol L^{-1})	240	0.2 ± 0.0	0.2 ± 0.0	0.2 ± 0.0	0.2 ± 0.0	Treatment	*n.s.*
	630	1.6 ± 0.4	1.6 ± 0.4	1.5 ± 0.3	1.5 ± 0.1	Time	***
	1000	1.4 ± 0.1	1.4 ± 0.1	1.4 ± 0.4	1.4 ± 0.1	Interaction	*n.s.*
	Average	1.0 ± 0.7A	1.1 ± 0.7A	1.0 ± 0.7A	1.0 ± 0.6A		
pH	240	6.7 ± 0.7	7.2 ± 0.4	6.5 ± 0.3	6.9 ± 0.6	Treatment	*n.s.*
	630	6.9 ± 0.3	6.7 ± 0.3	6.5 ± 0.9	6.5 ± 0.5	Time	*n.s.*
	1000	6.5 ± 0.8	6.1 ± 0.9	7.1 ± 0.2	6.8 ± 0.5	Interaction	*n.s.*
	Average	6.7 ± 0.6A	6.6 ± 0.7A	6.7 ± 0.6A	6.7 ± 0.5A		
Fe(III) (μmol g^{-1})	240	85.4 ± 5.2	77.5 ± 2.5	101.8 ± 13.2	88.1 ± 9.9	Treatment	***
	630	59.8 ± 8.9	56.5 ± 5.5	79.9 ± 12.9	67.5 ± 3.4	Time	***
	1000	72.1 ± 3.6	76.2 ± 14.3	100.9 ± 7.2	80.9 ± 3.1	Interaction	*n.s.*
	Average	72.4 ± 12.4B	70.1 ± 12.8B	94.2 ± 14.6A	78.8 ± 10.6AB		
Soil Fe(III)/Fe(II) ratios	240	2.6 ± 0.5	3.0 ± 0.1	3.9 ± 0.3	2.8 ± 0.6	Treatment	***
	630	1.9 ± 0.3	1.3 ± 0.2	2.8 ± 0.7	2.0 ± 0.2	Time	***
	1000	1.3 ± 0.3	2.2 ± 0.4	2.9 ± 0.2	2.0 ± 0.3	Interaction	*n.s.*
	Average	1.9 ± 0.6B	2.2 ± 0.8B	3.2 ± 0.6A	2.3 ± 0.5AB		
Dissolved organic C (mg kg^{-1})	240	289.4 ± 43.2	362.2 ± 80.6	480.9 ± 35.6	481.1 ± 70.5	Treatment	***
	630	311.0 ± 37.5	313.4 ± 40.7	567.9 ± 39.9	483.8 ± 62.0	Time	*n.s.*
	1000	403.1 ± 66.2	402.0 ± 124.9	608.9 ± 159.6	494.1 ± 107.1	Interaction	*n.s.*
	Average	334.5 ± 68.2C	347.2 ± 77.3C	552.6 ± 101.4AB	486.4 ± 71.4B		
NO_3^- (mg kg^{-1})	240	2.3 ± 1.0	4.7 ± 1.0	1.9 ± 1.3	3.1 ± 0.3	Treatment	***
	630	2.4 ± 0.5	5.0 ± 0.5	1.9 ± 0.8	3.9 ± 0.7	Time	*
	1000	1.6 ± 0.2	3.6 ± 0.5	1.7 ± 0.8	2.7 ± 0.2	Interaction	*n.s.*
	Average	2.1 ± 0.7C	4.4 ± 0.9A	1.8 ± 0.9C	3.2 ± 0.7B		
NH_4^+ (mg kg^{-1})	240	24.9 ± 2.7	33.2 ± 5.2	32.1 ± 5.2	21.1 ± 3.2	Treatment	***
	630	23.1 ± 8.4	32.6 ± 4.7	29.6 ± 7.9	42.5 ± 11.2	Time	*n.s.*
	1000	18.6 ± 3.7	47.1 ± 4.3	22.9 ± 6.3	36.1 ± 11.7	Interaction	**
	Average	22.2 ± 5.6C	37.6 ± 8.2A	28.2 ± 7.0 BC	33.2 ± 12.6AB		
TN (g kg^{-1})	240	2.1 ± 0.1	2.3 ± 0.0	1.9 ± 0.1	2.3 ± 0.0	Treatment	***
	630	2.3 ± 0.1	2.9 ± 0.2	2.5 ± 0.2	2.9 ± 0.2	Time	***
	1000	2.3 ± 0.2	3.0 ± 0.2	2.5 ± 0.2	3.0 ± 0.4	Interaction	*n.s.*
	Average	2.2 ± 0.2B	2.7 ± 0.3A	2.3 ± 0.4B	2.7 ± 0.4A		
C/N ratios	240	9.2 ± 0.4	8.0 ± 0.4	10.9 ± 1.0	8.4 ± 0.7	Treatment	***
	630	8.8 ± 1.1	7.0 ± 1.3	7.9 ± 0.7	7.3 ± 0.8	Time	***

(Continues)

Table 1. Continued

Variables	Time (d)	Treatments					
		Control	N	I	N + I		*p*
	1000	8.6 ± 0.7	6.7 ± 0.6	8.4 ± 0.4	7.1 ± 1.1	Interaction	*n.s.*
	Average	8.9 ± 0.7A	7.2 ± 1.0B	9.1 ± 1.5A	7.6 ± 1.0B		

n.s., not significant; *$p < 0.05$, **$p < 0.01$, and ***$p < 0.001$. Different capital letters indicate significant differences across treatments.

and microbial drivers (40%), with plant drivers contributing 18%. For Fe-OC, edaphic drivers were most influential (55%), while microbial drivers accounted for 35% and plant drivers 10%. The Random Forest modeling revealed that fungal/bacterial ratios, phenol oxidase, and β-1,4-glucosidase activities were the dominant factors affecting POC (Fig. 4a). In contrast, the primary drivers for MAOC were fungal necromass C, belowground biomass, and soil Fe(III) concentrations (Fig. 4b). For Fe-OC, soil Fe(III) concentrations were identified as the key drivers (Fig. 4c). Specifically, POC was negatively associated with fungal/bacterial ratios, phenol oxidase activities, and β-1,4-glucosidase activities (Fig. 4d–f). Conversely, MAOC was positively correlated with belowground biomass, fungal necromass C, and soil Fe(III) concentrations (Fig. 4g–i).

We performed SEM to further explore how N loading and increased inundation regulate SOC stabilization (Fig. 5a). Our initial SEM considered how N loading and increased inundation affected edaphic conditions [soil Fe(III)], belowground biomass, and microbial properties (including fungal necromass C, fungal/bacterial ratios, and phenol oxidase activities), with these three factor categories then influencing SOC stabilization (Supporting Information Fig. S2). However, this initial model did not achieve a satisfactory fit ($p < 0.05$). According to our Random Forest modeling, SOC fractions were strongly driven by soil Fe(III) concentrations, fungal necromass C, fungal/bacterial ratios, phenol oxidase, and belowground biomass (Fig. 4a–i), prompting us to construct a revised path-analysis model. Therefore, in the refined model, we positioned N loading and increased inundation as first-tier factors, fungal/bacterial ratios and belowground biomass as second-tier factors, which in turn influenced C-acquiring enzyme activities, fungal necromass C, and soil Fe(III) as third-tier factors, ultimately affecting SOC stabilization (fourth tier). We achieved the final model by eliminating direct pathways from N loading and sea-level rise to SOC stabilization, as well as removing direct effects from fungal/bacterial ratios and belowground biomass (Supporting Information Fig. S3). Our final model demonstrated excellent fit statistics (Fisher's $C = 80.16$, $df = 28$, $p = 0.104$, $AIC = 155$). Specifically, N loading reduced fungal/bacterial ratios (path coefficient = −0.30), which were positively associated with both C-acquiring enzyme activities (0.51) and fungal necromass C (0.53). Conversely, increased inundation enhanced belowground biomass (0.64), which positively influenced soil Fe(III) (0.63) and C-acquiring enzyme activities (0.33). Fungal necromass C (0.35), C-acquiring enzyme activities (0.39), and soil Fe(III) (0.39) influenced SOC stabilization. This optimized SEM successfully captured the relationships between our variables of interest, revealing that N loading had a negative effect (−0.12) on SOC stabilization, whereas increased inundation had a positive influence (0.24) (Fig. 5b).

Discussion

Individual effect of nitrogen loading on soil organic carbon stabilization

Consistent with our Hypothesis I, N loading decreased SOC stabilization (Fig. 3b), resulting from an increase in POC (Fig. 2a) and a decrease in MAOC (Fig. 2b). However, the underlying mechanisms differed partially from our initial hypothesis. Contrary to our hypothesis that N loading would increase POC through enhancing plant biomass, we found no significant changes in either above- or belowground biomass under N loading (Table 2). This unexpected finding indicated our study site was not N-limited, differing from many tidal marshes but aligning with P limitation commonly observed in subtropical tidal marshes (Fan et al. 2023). Instead, our Random Forest analysis identified fungal/bacterial ratios and phenol oxidase activity as the primary factors influencing POC (Fig. 4a). Structural equation modeling analyses revealed that N loading shifted microbial community composition from fungal to bacterial dominance (Fig. 5a), a change attributed to the competitive advantage bacteria (copiotrophs) gain over fungi (oligotrophs) in N-enriched environments (Norris et al. 2021; Wang et al. 2021b). The decreased fungal/bacterial ratios strongly correlated with reduced oxidative enzyme activity (Fig. 5a; Supporting Information Fig. S4b), which was consistent with fungi being the primary producers of this enzyme (Sinsabaugh 2010; Zavarzina et al. 2018). As phenol oxidase degrades lignin-rich compounds that constitute the majority of POC (Sinsabaugh 2010), the reduction in this enzyme activity significantly impaired POC decomposition processes. Therefore, despite unchanged plant inputs, this impaired decomposition pathway resulted in POC accumulation under N loading conditions (Liang et al. 2021).

Consistent with our hypothesis that N loading would decrease MAOC through reduced fungal necromass contribution, SEM analyses confirmed a significant relationship

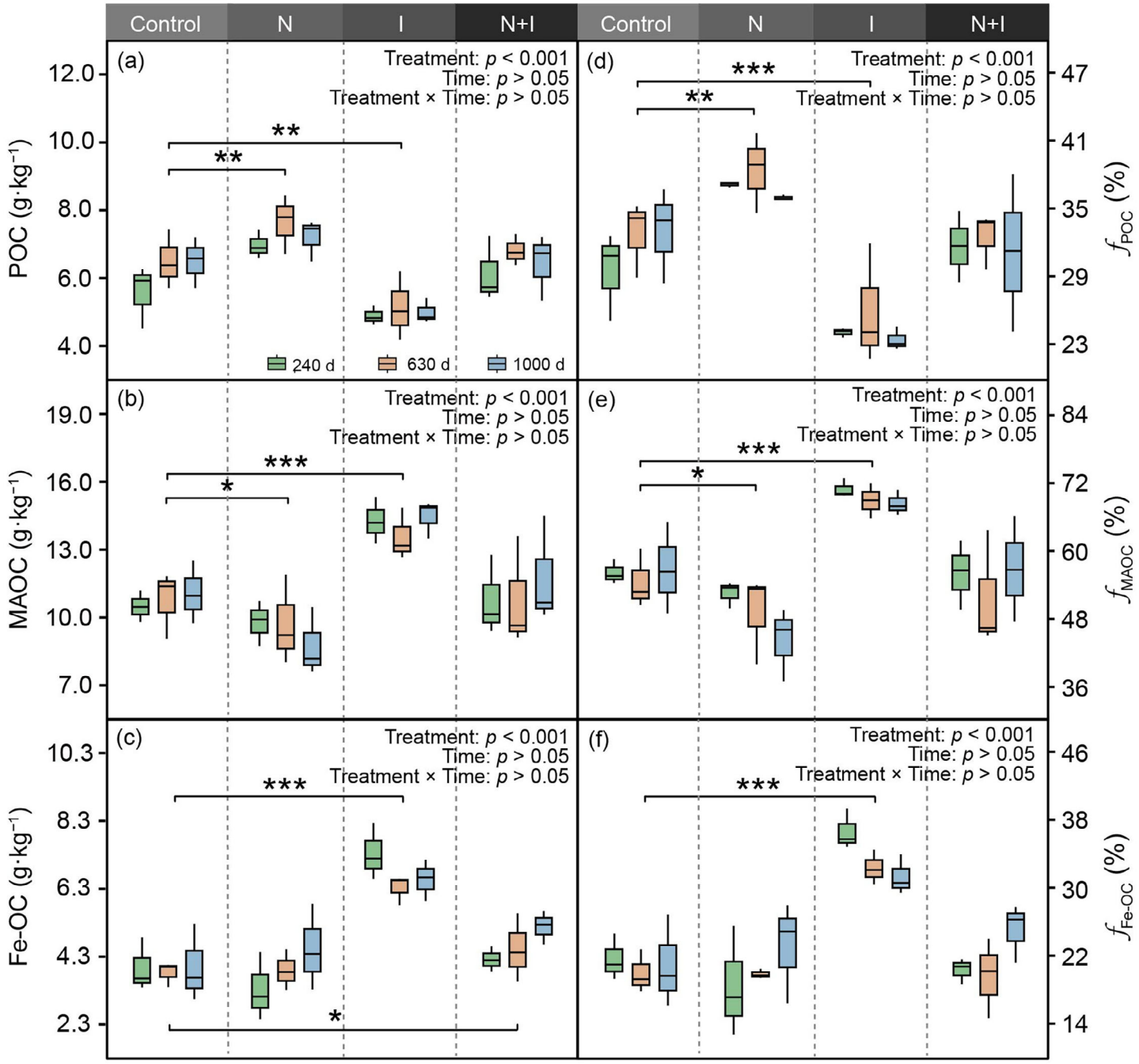


Fig. 2. Soil organic carbon fractions. Effects of nitrogen loading, increased inundation, and their combined impact on SOC fractions (**a**–**c**) and their proportions in total SOC (**d**–**e**). A linear mixed-effects (LME) model was used to estimate the effect of treatments and sampling times on SOC fractions and their proportions. Treatments and times were treated as fixed factors, and the plots were hierarchically arranged as random factors. When the LME's results showed significant differences, a least-significant-difference (LSD) test was conducted to elucidate multiple comparisons. Asterisks denote significant differences across treatments (*$p < 0.05$; **$p < 0.01$; ***$p < 0.001$). SOC: soil organic carbon; POC: particulate organic carbon; MAOC: mineral-associated organic carbon; Fe-OC: iron-bound organic carbon. f_{POC}: the proportion of POC in SOC; f_{MAOC}: the proportion of MAOC in total SOC; $f_{Fe\text{-}OC}$: the proportion of Fe-OC in SOC; N: nitrogen loading; I: increased inundation; N + I: combination of nitrogen loading and increased inundation.

between decreased fungal/bacterial ratios and reduced SOC stabilization (Fig. 5a,b). The fungal/bacterial ratios strongly correlated with fungal necromass production (Fig. 5a; Supporting Information Fig. S4a). This relationship operates through the "microbial carbon pump" mechanism (Liang 2020), whereby soil microorganisms transform plant-derived C into microbial biomass through metabolic processes, which subsequently becomes microbial necromass

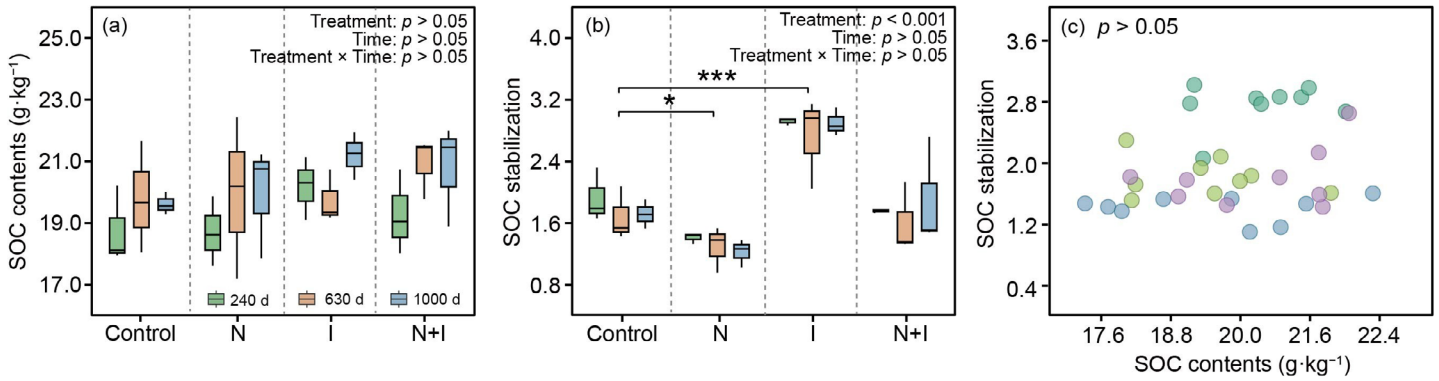


Fig. 3. Soil organic carbon contents and stabilization. Effects of nitrogen loading, increased inundation, and their combined impact on SOC contents and stabilization (**a**, **b**) and the relationships among these two variables (**c**). A linear mixed-effects (LME) model was used to estimate the effect of treatments and sampling times on SOC contents and stabilization (a, b). Treatments and times were treated as fixed factors, and the plots were hierarchically arranged as random factors. When the LME's results showed significant differences, a least-significant-difference (LSD) test was conducted to elucidate multiple comparisons. Asterisks denote significant differences across treatments (*$p < 0.05$; **$p < 0.01$; ***$p < 0.001$). SOC stabilization: the ratio of MAOC to POC; N: nitrogen loading; I: increased inundation; N + I: combination of nitrogen loading and increased inundation.

upon cell death (Sokol and Bradford 2019; Lavallee et al. 2020; Li et al. 2022). In our control treatment, fungal necromass exceeded bacterial necromass approximately eight-fold (Table 2), attributable to fungi's greater biomass and extended lifespan (Mou et al. 2021). Consequently, the substantial decrease in fungal necromass outweighed the unchanged bacterial necromass under N enrichment (Table 2). This reduction in fungal/bacterial ratios under N loading significantly diminished the total microbial necromass available for mineral interaction, thereby reducing MAOC formation (Sokol and Bradford 2019).

In summary, N loading decreased SOC stabilization primarily through altering microbial community composition—specifically reducing fungal/bacterial ratios—which simultaneously increased POC through reduced oxidative enzyme activity and decreased MAOC through diminished fungal necromass production. These results highlighted the critical role of microbial community composition in mediating soil C dynamics in tidal marshes under N loading in non-N limited tidal marsh systems.

Individual effect of increased inundation on soil organic carbon stabilization

Contradicting Hypothesis II, our results showed that increased inundation enhanced SOC stabilization (Fig. 3b), resulting from a decrease in POC (Fig. 2a) and an increase in MAOC (Fig. 2b). Contrary to our hypothesis that increased inundation would promote POC accumulation through suppressed oxidative enzyme activities under anaerobic conditions, we observed a significant decrease in POC (Fig. 2a), accompanied by an increase in phenol oxidase activity (Table 2). The plant adaptation response to inundation could provide a mechanistic explanation for these unexpected results. The soil Fe(III)/Fe(II) ratios increased significantly under inundation conditions (Table 1), indicating enhanced root oxygen loss despite elevated water levels—a phenomenon previously documented in the plant species present at our study site (Hu et al. 2023). This occurred because vascular wetland plants adapt to inundation by increasing belowground biomass (Table 2) and thereby enhancing oxygen transport through root aerenchyma (Armstrong et al. 2000; Liu et al. 2021). This process, known as root oxygen loss, produces oxidizing agents such as hydroxyl radicals (·HO), O_2, and H_2O_2 in the rhizosphere (Fenner and Freeman 2011; Yu and Kuzyakov 2021), which directly stimulate phenol oxidase activity (Fig. 5a), as these enzymes require oxygen to function effectively. As proof, we found increased phenol oxidase activity (Table 2). This enhancement in oxidative enzyme function accelerated POC decomposition, consequently reducing POC concentrations rather than promoting their accumulation as initially hypothesized.

The observed increase in MAOC under inundation supported the alternative mechanism mentioned in our introduction regarding Fe-OC associations. Our results showed soil Fe(III) concentrations increased significantly under inundation (Table 1), which strongly correlated with MAOC (Fig. 4i). The increased oxidizing agents in the soils not only stimulated phenol oxidase activity but also promoted Fe(III) precipitation (Naughton et al. 2023). These Fe(III) minerals generally form around marsh plant roots with larger specific surface areas, which stabilized labile C compounds (e.g., root exudates) through adsorption, facilitating Fe-OC associations (Lalonde et al. 2012; Jeewani et al. 2020). Unlike our findings with N loading, we did not observe significant changes in fungal necromass C under increased inundation (Table 2), indicating that changes in microbial necromass played an unimportant role in MAOC enhancement in this treatment. This result suggested that the mineral-associated pathway, particularly Fe-

Table 2. Effects of nitrogen loading (N), increased inundation (I), and the combination of nitrogen loading and increased inundation (N + I) on plant biomass and microbial properties at 240 d, 630 d, and 1000 d (n = 3). N: nitrogen loading; I: increased inundation; N + I: combination of nitrogen loading and increased inundation.

		Treatments					
Variables	**Time (d)**	**Control**	**N**	**I**	**N + I**		***p***
Aboveground biomass (kg m^{-2})	240	4.2 ± 1.7	4.7 ± 1.3	4.3 ± 0.7	5.0 ± 0.8	Treatment	*n.s.*
	630	4.3 ± 1.0	4.3 ± 0.9	3.8 ± 0.6	3.4 ± 0.5	Time	*n.s.*
	1000	4.3 ± 1.5	4.5 ± 1.2	4.0 ± 0.5	4.2 ± 0.7	Interaction	*n.s.*
	Average	4.3 ± 1.2A	4.5 ± 1.0A	4.0 ± 0.5A	4.2 ± 0.9A		
Belowground biomass (kg m^{-2})	240	1.9 ± 0.4	1.6 ± 0.1	3.2 ± 0.7	1.9 ± 0.4	Treatment	***
	630	2.1 ± 0.3	2.0 ± 0.5	3.3 ± 0.4	2.5 ± 0.5	Time	**
	1000	2.2 ± 0.1	2.4 ± 0.6	2.9 ± 0.2	2.5 ± 0.5	Interaction	*n.s.*
	Average	2.1 ± 0.3B	2.0 ± 0.5B	3.1 ± 0.4A	2.3 ± 0.5AB		
Fungal biomass (nmol g^{-1})	240	0.3 ± 0.1	0.2 ± 0.0	0.4 ± 0.0	0.2 ± 0.0	Treatment	*
	630	0.3 ± 0.0	0.3 ± 0.1	0.4 ± 0.2	0.3 ± 0.1	Time	*n.s.*
	1000	0.4 ± 0.0	0.3 ± 0.0	0.3 ± 0.1	0.4 ± 0.0	Interaction	*n.s.*
	Average	0.3 ± 0.1A	0.3 ± 0.1B	0.4 ± 0.1A	0.3 ± 0.1AB		
Bacterial biomass (nmol g^{-1})	240	2.6 ± 0.2	3.0 ± 0.2	2.0 ± 0.3	1.8 ± 0.2	Treatment	***
	630	2.8 ± 0.2	4.9 ± 1.2	1.9 ± 0.4	2.0 ± 0.3	Time	***
	1000	3.5 ± 0.2	5.0 ± 0.7	2.4 ± 0.4	2.6 ± 0.3	Interaction	*n.s.*
	Average	3.0 ± 0.5B	4.3 ± 1.2A	2.1 ± 0.4C	2.1 ± 0.5C		
Fungal/bacterial ratios	240	0.1 ± 0.0	0.1 ± 0.0	0.2 ± 0.0	0.1 ± 0.0	Treatment	***
	630	0.1 ± 0.0	0.1 ± 0.0	0.2 ± 0.1	0.2 ± 0.0	Time	*n.s.*
	1000	0.1 ± 0.0	0.1 ± 0.0	0.1 ± 0.0	0.1 ± 0.0	Interaction	*n.s.*
	Average	0.1 ± 0.0AB	0.1 ± 0.0B	0.2 ± 0.1A	0.1 ± 0.0AB		
Fungal necromass C (g kg^{-1})	240	3.5 ± 0.2	3.1 ± 0.4	3.6 ± 0.3	3.4 ± 0.2	Treatment	***
	630	3.5 ± 0.4	2.3 ± 0.4	3.4 ± 0.4	3.0 ± 0.3	Time	***
	1000	3.0 ± 0.3	1.9 ± 0.3	3.4 ± 0.3	2.4 ± 0.8	Interaction	*n.s.*
	Average	3.3 ± 0.4AB	2.5 ± 0.6C	3.5 ± 0.3A	2.9 ± 0.6 BC		
Bacterial necromass C (g kg^{-1})	240	0.5 ± 0.2	0.5 ± 0.2	0.4 ± 0.0	0.3 ± 0.0	Treatment	*
	630	0.4 ± 0.1	0.2 ± 0.1	0.2 ± 0.0	0.3 ± 0.0	Time	*
	1000	0.4 ± 0.2	0.4 ± 0.1	0.3 ± 0.1	0.3 ± 0.1	Interaction	*n.s.*
	Average	0.4 ± 0.1A	0.4 ± 0.2AB	0.3 ± 0.1B	0.3 ± 0.1B		
β-1,4-glucosidase (nmol g^{-1} h^{-1})	240	3.5 ± 0.7	3.4 ± 1.0	3.7 ± 0.5	3.3 ± 0.7	Treatment	***
	630	3.7 ± 1.0	3.3 ± 0.7	5.4 ± 1.7	4.5 ± 0.7	Time	***
	1000	2.7 ± 0.8	3.4 ± 0.1	4.1 ± 0.6	3.2 ± 1.1	Interaction	*n.s.*
	Average	3.3 ± 0.9B	3.4 ± 0.6B	4.4 ± 1.2A	3.7 ± 1.0B		
Phenol oxidase (nmol g^{-1} h^{-1})	240	76.1 ± 18.1	47.7 ± 9.7	125.0 ± 51.2	54.1 ± 15.3	Treatment	***
	630	81.0 ± 4.1	32.1 ± 11.4	140.8 ± 43.7	81.0 ± 13.6	Time	*n.s.*
	1000	68.1 ± 14.2	39.3 ± 11.0	119.8 ± 50.5	55.7 ± 12.7	Interaction	*n.s.*
	Average	75.1 ± 12.9B	39.7 ± 11.5C	128.6 ± 43.1A	63.6 ± 17.7B		

n.s., not significant; *$p < 0.05$, **$p < 0.01$, and ***$p < 0.001$. Different capital letters indicate significant differences across treatments.

OC associations, was the dominant mechanism for enhanced MAOC formation under increased inundation.

In summary, increased inundation enhanced SOC stabilization primarily by altering plant C allocation patterns—specifically increasing belowground biomass and oxygen transport—which simultaneously decreased POC through enhanced oxidative enzyme activity and increased MAOC through elevated Fe(III) concentrations and Fe-OC associations. These results highlighted the important but often overlooked role of plant adaptations in mediating soil C responses to inundation in tidal marsh ecosystems.

Combined effect of nitrogen loading and increased inundation on soil organic carbon stabilization

Contrary to Hypothesis III, our results demonstrated that the combined N loading and increased inundation resulted in no

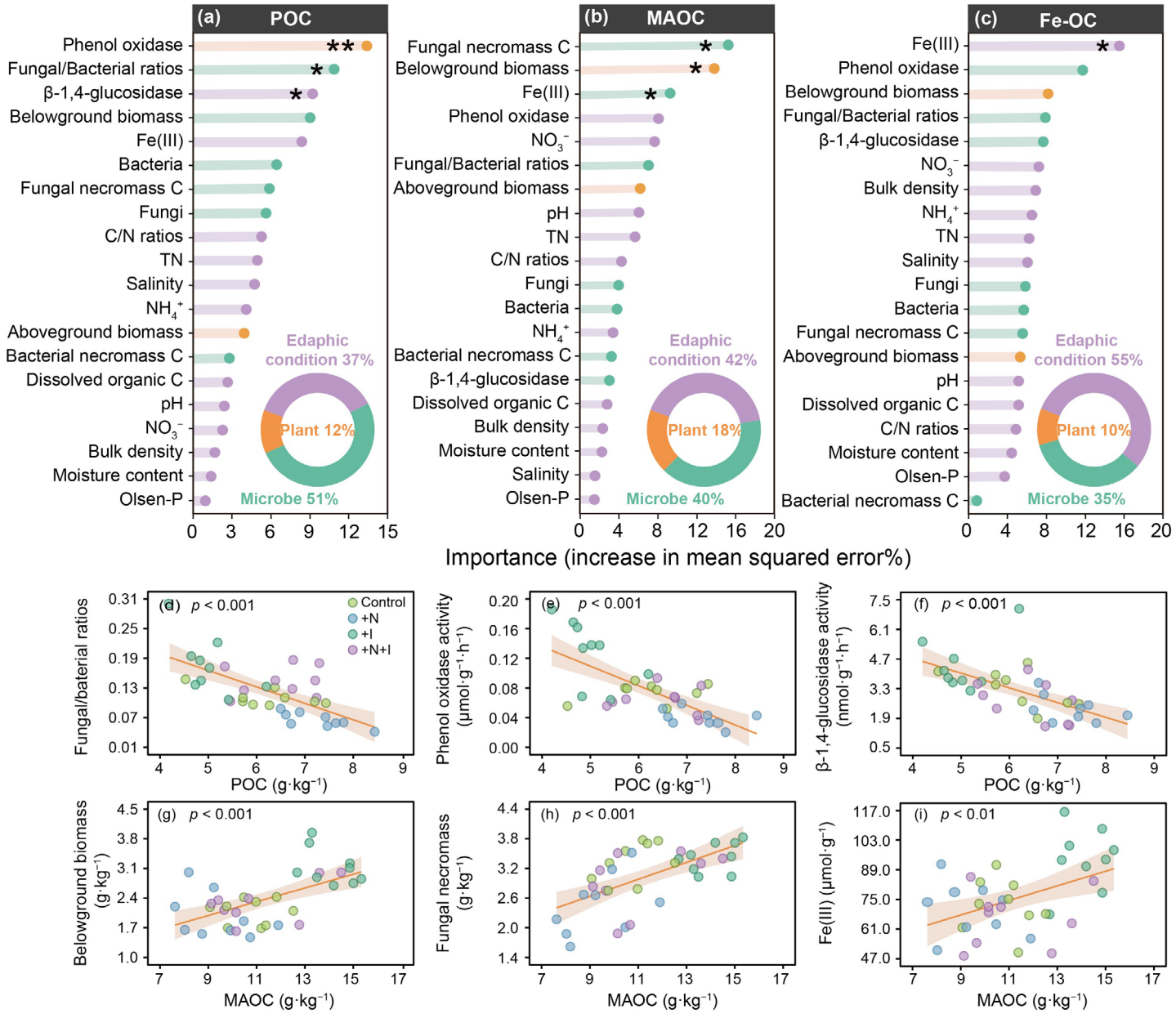


Fig. 4. Environmental drivers of soil organic carbon fractions. Random Forest model evaluated the importance (percentage increase in the mean squared error) of edaphic, plant, and microbial variables as drivers of SOC fractions (**a–c**). Relationship between SOC fractions and selected drivers (**d–i**). The orange, purple, and green in panels (a–c) represent plant, edaphic, and microbial variables, respectively. Significance levels are as follows: *$p < 0.05$; **$p < 0.01$; ***$p < 0.001$. POC: particulate organic carbon; MAOC: mineral-associated organic carbon; Fe-OC: iron-bound organic carbon; N: nitrogen loading; I: increased inundation; N + I: combination of nitrogen loading and increased inundation.

significant changes in either POC or MAOC compared to the control treatment (Fig. 2a,b). Consequently, SOC stabilization was maintained at control levels despite the dual stressors (Fig. 3b). Our Random Forest analysis identified soil C-acquiring enzyme activities as the primary factors influencing POC (Fig. 4a). When examining individual treatments, N loading significantly reduced phenol oxidase activity, leading to POC accumulation, while increased inundation enhanced phenol oxidase activities, resulting in POC reduction (Fig. 6a,b). Remarkably, under the combined N + I treatment, the enzyme activities showed no significant differences from control conditions (Table 2), confirming that the stimulatory effect of increased inundation on oxidative enzyme activity effectively counterbalanced the inhibitory effect of N loading (Fig. 6c). This enzymatic equilibrium under combined treatments explained why POC remained at levels similar to the control treatment.

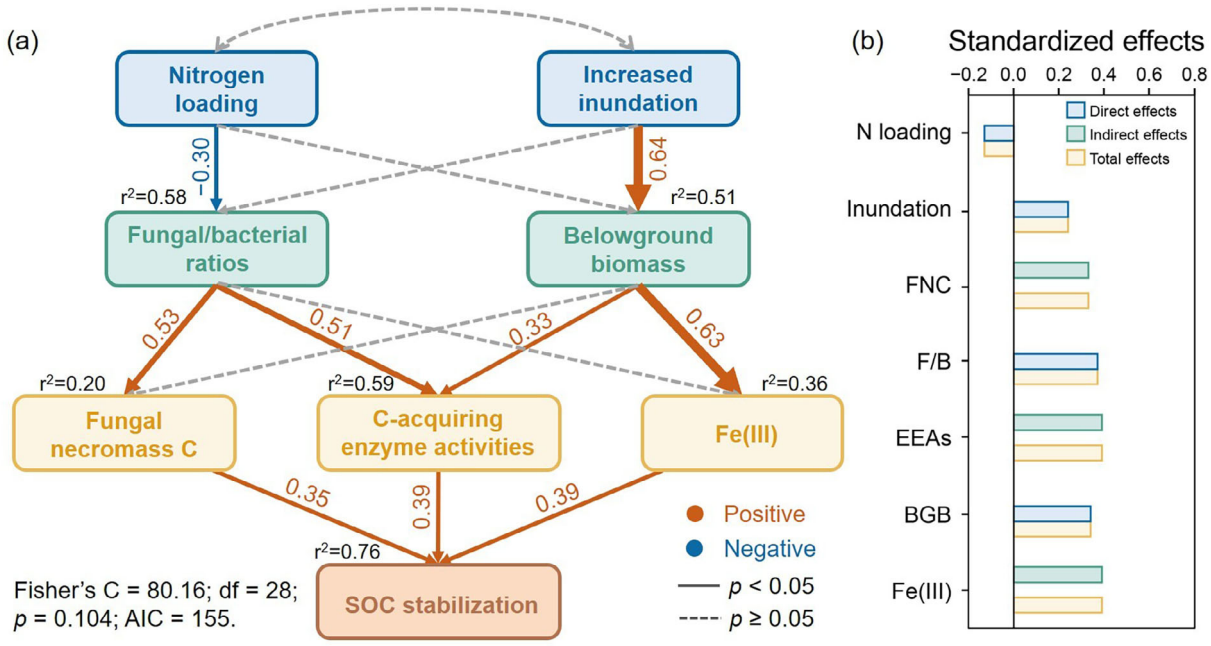


Fig. 5. Impact of nitrogen loading and increased inundation on soil organic carbon stabilization. Structural equation modeling outcomes of expected causal relationships (**a**). The standardized effects on the SOC stabilization (**b**). Arrows in panel (a) indicate the hypothesized direction of causation. Red and blue solid arrows in panel (a) reflect positive and negative relationships, respectively. The width of arrows is proportional to the strength of the relationship. The numbers adjacent to the arrows in panel (a) are the standardized path coefficients. The dotted arrows in panel (a) indicate insignificant relationships. r^2 indicates the proportion of variations explained for the dependent variable. SOC: soil organic carbon; Fe(III): iron oxides; FNC: fungal necromass carbon; EEAs: extracellular enzyme activities; BGB: belowground biomass; F/B: fungal/bacterial ratios.

Mineral-associated organic carbon likewise showed no significant change under combined treatments, but through different counteracting mechanisms (Fig. 6c). Our results revealed that N loading decreased fungal necromass C, a key contributor to MAOC formation (Table 2). Meanwhile, increased inundation promoted Fe-OC associations that contribute to MAOC (Fig. 2c). Under the combined treatment, fungal necromass C remained significantly lower than control, similar to the N treatment alone (Table 2), whereas Fe-OC levels remained significantly elevated compared to control treatment (Fig. 2c). Our results suggested that the increase in Fe-OC associations under combined treatments effectively compensated for the decrease in fungal necromass C, resulting in MAOC levels comparable to control (Fig. 6c).

In summary, our results demonstrate that when N loading and increased inundation occur simultaneously, their opposing effects on key soil processes create a counterbalancing effect that maintains SOC stabilization at levels similar to undisturbed conditions. This unexpected outcome highlights the importance of multifactor experiments in predicting ecosystem responses to concurrent global change drivers, as interactive effects can differ substantially from predictions based on single-factor studies.

Implication for future management under global changes

In our study, we discovered that despite no significant changes in total SOC contents under our two global change treatments (Fig. 3a), SOC stability exhibited substantial variations (Fig. 3b). We found no inherent correlation between stability and contents (Fig. 3c). The counteracting effects of N loading and increased inundation suggested that in regions experiencing both sea-level rise and N enrichment, the impact on SOC dynamics may be less detrimental than initially anticipated compared to areas exposed to only one of these global changes (Knorr et al. 2024). This insight offers new directions for developing targeted management strategies in tidal marsh ecosystems affected by different combinations of global change factors. For tidal marshes facing substantial N loading, hydrological management approaches could help mitigate negative effects on SOC stabilization. Strategies such as dike removal, surface elevation adjustments, tidal exchange restoration, and introducing freshwater through artificial channels could increase inundation and thus promote SOC stabilization by enhancing oxidative enzyme activity and Fe-OC associations (Ji et al. 2024). Conversely, in tidal marshes experiencing rapid sea-level rise without significant N enrichment, carefully increasing nutrient inputs could help protect vulnerable unstable C, thereby supporting overall SOC preservation (Zang et al. 2024).

Knowledge gaps and future research priorities

Despite the insights gained from this study, several knowledge gaps remain that warrant further investigation. First, while our multifactor design with a single N loading and

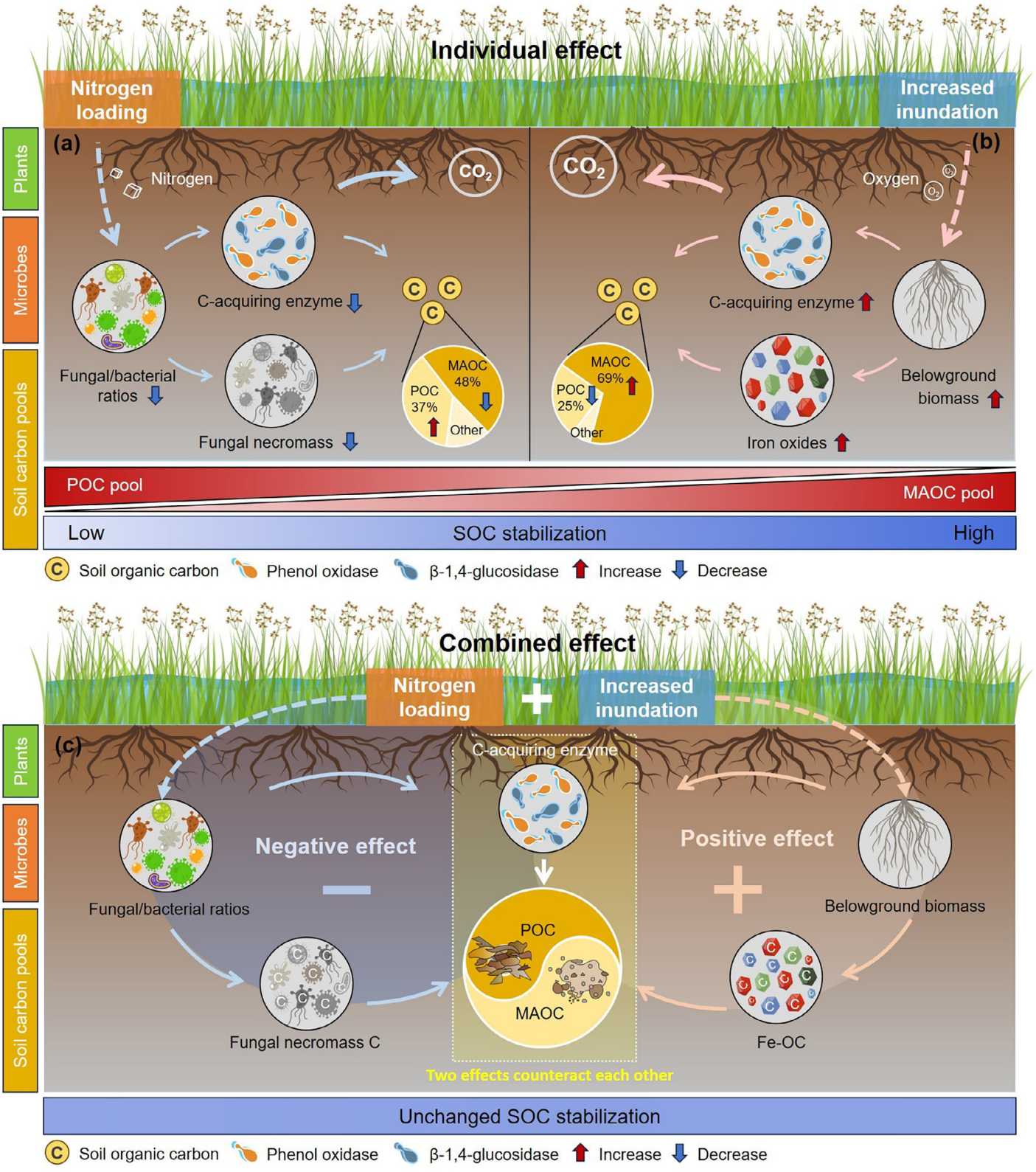


Fig. 6. Conceptual diagram illustrating the mechanisms by which nitrogen loading, increased inundation, and their combined effects influence soil organic carbon stabilization in a subtropical tidal marsh. (**a**) Individual effect of nitrogen loading on soil carbon cycling. (**b**) Individual effect of increased inundation on soil carbon cycling. (**c**) Combined effect of nitrogen loading and increased inundation on soil carbon cycling. POC: particulate organic carbon; MAOC: mineral-associated organic carbon; Fe-OC: iron-bound organic carbon; SOC: soil organic carbon.

inundation level simplified the analysis of independent factors, this approach may not fully capture the complexity of natural ecosystems (Kleine et al. 2021; Chen et al. 2022; Hu et al. 2023). Future research should incorporate multiple gradients of N loading and inundation to better understand potential threshold effects and non-linear responses. Second, N deposition in natural systems typically consists of chronic, low-dose inputs, unlike the high-pulse N inputs in our experiment. Research has shown that ecosystems respond differently to continuous, low-dose inputs compared to sporadic, high-pulse inputs (Cao et al. 2020). Therefore, future studies should investigate the long-term effects of various N loading patterns on tidal marsh carbon dynamics. Third, our experiment employed passive weirs to assess the impact of increased inundation on SOC stabilization, which extended inundation frequency but did not raise inundation depth. Considering the potential effects of inundation depth on plant growth and photosynthetic conditions, we recommend utilizing active weirs (increasing both inundation frequency and depth) in future work (Cherry et al. 2015). Fourth, our experiment lasted only 3 yr, which may be insufficient to capture the full ecosystem response. Both plants and soil microorganisms require longer periods to acclimate to environmental changes (Kleine et al. 2021). The short-term duration limited our ability to thoroughly evaluate the long-term effects of N loading and increased inundation on soil C cycling in tidal marsh ecosystems (Averill and Waring 2018). Finally, our study was conducted at a single subtropical tidal marsh site with phosphorus limitation, which differs from many nitrogen-limited tidal marshes globally. Multi-site experiments across different geographic regions and nutrient limitation conditions would provide more comprehensive insights into the interactive effects of global change factors on blue carbon ecosystems. Despite these knowledge gaps, our results demonstrated distinct differences in SOC stabilization mechanisms within tidal marshes under N loading, increased inundation, and their combination. These findings underscore the necessity for targeted management strategies and further research to effectively conserve these valuable blue carbon ecosystems under multiple global change drivers.

Conclusion

Our 3-yr in situ experiment has unveiled novel insights into the complex dynamics of SOC stabilization in response to N loading and increased inundation in a subtropical tidal marsh. Our findings highlighted that N loading increased POC and decreased MAOC, thereby decreasing SOC stabilization. In contrast, increased inundation raised MAOC and reduced POC, leading to an increase in SOC stabilization. Interestingly, the combined effect of N loading and increased inundation had no significant impact on SOC stabilization, challenging conventional assumptions about the additive effects of multiple stressors. This unexpected finding suggested that in regions facing both sea-level rise and N enrichment, SOC storage and its stabilization may be less adversely affected than initially expected, especially compared to areas experiencing only one of these global changes. The combined effects of these two global change drivers produced a unique response that could not be predicted from their individual impacts alone, underscoring the complexity of ecosystem responses to multiple environmental pressures. Our findings underscore the critical necessity of multifactor experiments for accurately predicting soil C dynamics in an era when tidal ecosystems simultaneously face numerous global change stressors, while also establishing a novel framework for understanding and enhancing coastal wetland resilience under accelerating environmental change.

Author Contributions

Tianning Fan: Formal analysis, investigation, writing – original draft. Jiafang Huang: Investigation, funding acquisition. Guopeng Liang: Writing – review & editing. Shengen Liu: Writing – review & editing. Dehong Hu: Formal analysis, investigation. Lifei Su: Formal analysis, investigation. Yi Liu: Formal analysis, investigation. YuanBin Cai: Formal analysis, investigation. Shihua Li: Formal analysis, investigation. Pingping Guo: Investigation. Min Luo: Conceptualization, methodology, formal analysis, writing – original draft, writing – review & editing, supervision, funding acquisition, project administration. Chuan Tong: Conceptualization, project administration, supervision, funding acquisition.

Acknowledgments

We would like to thank the Katherine Rocci for her comments on earlier version of the manuscript. This work was financially supported by grants from the National Science Foundation of China (42177213; 32471672; 32071598), the Natural Science Foundation of Fujian Province (2024J01274; 2020J01503), the Fujian Minjiang River Estuary Wetland National Nature Reserve Administrative Office (MJHKSD20230202), the Study on "the Current Status of Blue Carbon Sequestration and Carbon Trade in the Coastal Wetlands of Fuzhou City" (No. [350182]FJYHZB[GK]2024001), the Science and Technology Projects of the Forest Bureau of Fujian Province (2021FKJ30), and the Public Welfare Project of Science and Technology Department of Fujian Province (2022R1002007).

Conflicts of Interest

None declared.

References

Appuhn, A., E. Scheller, and R. G. Joergensen. 2006. "Relationships Between Microbial Indices in Roots and Silt Loam Soils Forming a Gradient in Soil Organic Matter." *Soil*

Biology and Biochemistry 38: 2557–2564. https://doi.org/10.1016/j.soilbio.2006.03.011.

Angst, G., K. E. Mueller, K. G. J. Nierop, and M. J. Simpson. 2021. "Plant- or Microbial-Derived? A Review on the Molecular Composition of Stabilized Soil Organic Matter." *Soil Biology and Biochemistry* 156: 108189. https://doi.org/10.1016/j.soilbio.2021.108189.

Archer, E. 2016. rfPermute: Estimate Permutation *p*-Values for Random Forest Importance Metrics. https://CRAN.R-project.org/package=rfPermute.

Armstrong, W., D. Cousins, J. Armstrong, D. Turner, and P. Beckett. 2000. "Oxygen Distribution in Wetland Plant Roots and Permeability Barriers to Gas-Exchange with the Rhizosphere: A Microelectrode and Modelling Study with Phragmites Australis." *Annals of Botany* 86: 687–703. https://doi.org/10.1006/anbo.2000.1236.

Averill, C., and B. Waring. 2018. "Nitrogen Limitation of Decomposition and Decay: How Can It Occur?" *Global Change Biology* 24: 1417–1427. https://doi.org/10.1111/gcb.13980.

Bagnell, A., and T. DeVries. 2023. "Global Mean Sea Level Rise Inferred From Ocean Salinity and Temperature Changes." *Geophysical Research Letters* 50: e2022GL101004. https://doi.org/10.1029/2022GL101004.

Breitburg, D., L. A. Levin, A. Oschlies, et al. 2018. "Declining Oxygen in the Global Ocean and Coastal Waters." *Science* 359: eaam7240. https://doi.org/10.1126/science.aam7240.

Campbell, A. D. D., L. Fatoyinbo, L. Goldberg, and D. Lagomasino. 2022. "Global Hotspots of Salt Marsh Change and Carbon Emissions." *Nature* 612: 701–706. https://doi.org/10.1038/s41586-022-05355-z.

Cao, J., S. Pang, Q. Wang, et al. 2020. "Plant–Bacteria–Soil Response to Frequency of Simulated Nitrogen Deposition Has Implications for Global Ecosystem Change." *Functional Ecology* 34: 723–734. https://doi.org/10.1111/1365-2435.13484.

Chen, X., M. Luo, J. Tan, et al. 2022. "Salt-Tolerant Plant Moderates the Effect of Salinity on Soil Organic Carbon Mineralization in a Subtropical Tidal Wetland." *Science of the Total Environment* 837: 155855. https://doi.org/10.1016/j.scitotenv.2022.155855.

Cherry, J. A., G. S. Ramseur Jr., E. L. Sparks, and J. Cebrian. 2015. "Testing Sea-Level Rise Impacts in Tidal Marshes: A Novel In Situ Approach." *Methods in Ecology and Evolution* 6: 1443–1451. https://doi.org/10.1111/2041-210X.12441.

Cotrufo, M. F., and J. M. Lavallee. 2022. "Soil Organic Matter Formation, Persistence, and Functioning: A Synthesis of Current Understanding to Inform Its Conservation and Regeneration." In: Sparks, D.L. (Ed.), Advances in Agronomy. Cambridge, MA: Academic Press, pp. 1–66. https://doi.org/10.1016/bs.agron.2021.11.002.

Cotrufo, M. F., M. G. Ranalli, M. L. Haddix, J. Six, and E. Lugato. 2019. "Soil Carbon Storage Informed by Particulate and Mineral-Associated Organic Matter." *Nature Geoscience* 12: 989–994. https://doi.org/10.1038/s41561-019-0484-6.

Duarte, C. M., T. Sintes, and N. Marba. 2013. "Assessing the CO_2 Capture Potential of Seagrass Restoration Projects." *Journal of Applied Ecology* 50: 1341–1349. https://doi.org/10.1111/1365-2664.12155.

Fan, T., M. Luo, J. Tan, et al. 2023. "Incorporating Biotic Phosphorus-Acquisition Strategies Into Soil Phosphorus Transformation Under Long-Term Salinization in a Tidal Wetland." *Catena* 231: 107274. https://doi.org/10.1016/j.catena.2023.107274.

Fenner, N., and C. Freeman. 2011. "Drought-Induced Carbon Loss in Peatlands." *Nature Geoscience* 4: 895–900. https://doi.org/10.1038/ngeo1323.

Fortmann-Roe, S. 2013. Accurate, Adaptable, and Accessible Error Metrics for Predictive. R Package Version 0.9.2. https://cran.csail.mit.edu/web/packages/A3.

Freeman, C., N. Ostle, and H. Kang. 2001. "An Enzymic 'Latch' on a Global Carbon Store." *Nature* 409: 149. https://doi.org/10.1038/35051650.

Frostegård, Å., A. Tunlid, and E. Bååth. 2011. "Use and Misuse of PLFA Measurements in Soils." *Soil Biology and Biochemistry* 43: 1621–1625. https://doi.org/10.1016/j.soilbio.2010.11.021.

Hagh-Doust, N., V. Mikryukov, S. Anslan, et al. 2023. "Effects of Nitrogen Deposition on Carbon and Nutrient Cycling Along a Natural Soil Acidity Gradient as Revealed by Metagenomics." *New Phytologist* 238: 2607–2620. https://doi.org/10.1111/nph.18897.

Han, G., J. Li, and W. Qu. 2021. "Effects of Nitrogen Input on Carbon Cycle and Carbon Budget in a Coastal Salt Marsh." *Chinese Journal of Plant Ecology* 45: 321–333. https://doi.org/10.17521/cjpe.2020.0353.

Hu, D., W. Lan, M. Luo, et al. 2023. "Increase in Iron-Bound Organic Carbon Content under Simulated Sea-Level Rise: A 'Marsh Organ' Field Experiment." *Soil Biology & Biochemistry* 187: 109217. https://doi.org/10.1016/j.soilbio.2023.109217.

Huang, W., and S. J. Hall. 2017. "Elevated Moisture Stimulates Carbon Loss From Mineral Soils by Releasing Protected Organic Matter." *Nature Communications* 8: 1774. https://doi.org/10.1038/s41467-017-01998-z.

Jeewani, P. H., A. Gunina, L. Tao, et al. 2020. "Rusty Sink of Rhizodeposits and Associated Keystone Microbiomes." *Soil Biology & Biochemistry* 147: 107840. https://doi.org/10.1016/j.soilbio.2020.107840.

Ji, K., W. Ouyang, C. Lin, M. He, and X. Liu. 2024. "Eco-Hydrological Processes Regulate Lake Riparian Soil Organic Matter Under Dryness Stress." *Water Research* 260: 121938. https://doi.org/10.1016/j.watres.2024.121938.

Kleine, T., T. Nägele, H. E. Neuhaus, et al. 2021. "Acclimation in Plants—The Green Hub Consortium." *Plant Journal* 106: 23–40. https://doi.org/10.1111/tpj.15144.

Knorr, M. A., A. R. Contosta, E. W. Morrison, et al. 2024. "Unexpected Sustained Soil Carbon Flux in Response to Simultaneous Warming and Nitrogen Enrichment

Compared With Single Factors Alone." *Nature Ecology & Evolution* 8: 2277–2285. https://doi.org/10.1038/s41559-024-02546-x.

Kostka, J. E., and G. W. Luther. 1994. "Partitioning and Speciation of Solid Phase Iron in Saltmarsh Sediments." *Geochimica et Cosmochimica Acta* 58: 1701–1710. https://doi.org/10.1016/0016-7037(94)90531-2.

Lalonde, K., A. Mucci, A. Ouellet, and Y. Gelinas. 2012. "Preservation of Organic Matter in Sediments Promoted by Iron." *Nature* 483: 198–200. https://doi.org/10.1038/nature10855.

Lavallee, J. M., J. L. Soong, and M. F. Cotrufo. 2020. "Conceptualizing Soil Organic Matter into Particulate and Mineral-Associated Forms to Address Global Change in the 21st Century." *Global Change Biology* 26: 261–273. https://doi.org/10.1111/gcb.14859.

Lefcheck, J. S. 2016. "PIECEWISESEM: Piecewise Structural Equation Modelling in R for Ecology, Evolution, and Systematics." *Methods in Ecology and Evolution* 7: 573–579. https://doi.org/10.1111/2041-210X.12512.

Lehmann, J., C. M. Hansel, C. Kaiser, et al. 2020. "Persistence of Soil Organic Carbon Caused by Functional Complexity." *Nature Geoscience* 13: 529–534. https://doi.org/10.1038/s41561-020-0612-3.

Li, T., J. Zhang, X. Wang, I. P. Hartley, J. Zhang, and Y. Zhang. 2022. "Fungal Necromass Contributes More to Soil Organic Carbon and More Sensitive to Land Use Intensity Than Bacterial Necromass." *Applied Soil Ecology* 176: 104492. https://doi.org/10.1016/j.apsoil.2022.104492.

Liang, C. 2020. "Soil Microbial Carbon Pump: Mechanism and Appraisal." *Soil Ecology Letters* 2: 241–254. https://doi.org/10.1007/s42832-020-0052-4.

Liang, C., W. Amelung, J. Lehmann, and M. Kästner. 2019. "Quantitative Assessment of Microbial Necromass Contribution to Soil Organic Matter." *Global Change Biology* 25: 3578–3590. https://doi.org/10.1111/gcb.14781.

Liang, G., Y. Luo, Z. Zhou, and B. G. Waring. 2021. "Nitrogen Effects on Plant Productivity Change at Decadal Time-Scales." *Global Ecology and Biogeography* 30: 2488–2499. https://doi.org/10.1111/geb.13391.

Liaw, A., and M. Wiener. 2002. Classification and Regression by Random Forest. 2. https://journal.r-project.org/articles/RN-2002-022. https://doi.org/10.1046/j.1440-1746.17.s3.23.x.

Liu, Y., M. Luo, J. Chen, et al. 2021. "Root Iron Plaque Abundance as an Indicator of Carbon Decomposition Rates in a Tidal Freshwater Wetland in Response to Salinity and Flooding." *Soil Biology and Biochemistry* 162: 108403. https://doi.org/10.1016/j.soilbio.2021.108403.

Lugato, E., J. M. Lavallee, M. L. Haddix, P. Panagos, and M. F. Cotrufo. 2021. "Different Climate Sensitivity of Particulate and Mineral-Associated Soil Organic Matter." *Nature Geoscience* 14: 295–300. https://doi.org/10.1038/s41561-021-00744-x.

Luo, M., W. Zhu, J. Huang, et al. 2019. "Anaerobic Organic Carbon Mineralization in Tidal Wetlands Along a Low-Level Salinity Gradient of a Subtropical Estuary: Rates, Pathways, and Controls." *Geoderma* 337: 1245–1257. https://doi.org/10.1016/j.geoderma.2018.07.030.

Macreadie, P. I., T. B. Atwood, J. R. Seymour, et al. 2019. "Vulnerability of Seagrass Blue Carbon to Microbial Attack Following Exposure to Warming and Oxygen." *Science of the Total Environment* 686: 264–275. https://doi.org/10.1016/j.scitotenv.2019.05.462.

Macreadie, P. I., M. D. P. Costa, T. B. Atwood, et al. 2021. "Blue Carbon as a Natural Climate Solution." *Nature Reviews Earth and Environment* 2: 826–839. https://doi.org/10.1038/s43017-021-00224-1.

Mou, Z., L. Kuang, L. He, et al. 2021. "Climatic and Edaphic Controls Over the Elevational Pattern of Microbial Necromass in Subtropical Forests." *Catena* 207: 105707. https://doi.org/10.1016/j.catena.2021.105707.

Naughton, H. R., B. B. Tolar, C. Dewey, M. Keiluweit, P. S. Nico, and S. Fendorf. 2023. "Reactive Iron, Not Fungal Community, Drives Organic Carbon Oxidation Potential in Floodplain Soils." *Soil Biology and Biochemistry* 178: 108962. https://doi.org/10.1016/j.soilbio.2023.108962.

Norris, N., N. M. Levine, V. I. Fernandez, and R. Stocker. 2021. "Mechanistic Model of Nutrient Uptake Explains Dichotomy Between Marine Oligotrophic and Copiotrophic Bacteria." *PLoS Computational Biology* 17: e1009023. https://doi.org/10.1371/journal.pcbi.1009023.

Patzner, M. S., C. W. Mueller, M. Malusova, et al. 2020. "Iron Mineral Dissolution Releases Iron and Associated Organic Carbon During Permafrost Thaw." *Nature Communications* 11, no. 6329: 6329. https://doi.org/10.1038/s41467-020-20102-6.

Pinheiro, J., D. Bates, D. Sarkar, and R Development Core Team. 2011. nlme: Linear and Nonlinear Mixed Effects Models. R Package Version 3.1. https://cran.r-project.org/web//packages/nlme.

Rosseel, Y. 2012. "lavaan: An R Package for Structural Equation Modeling." *Journal of Statistical Software* 48, no. 1: 1–36. https://doi.org/10.18637/jss.v048.i02.

Saiya-Cork, K. R., R. L. Sinsabaugh, and D. R. Zak. 2002. "The Effects of Long Term Nitrogen Deposition on Extracellular Enzyme Activity in an Acer Saccharum Forest Soil." *Soil Biology and Biochemistry* 34: 1309–1315. https://doi.org/10.1016/S0038-0717(02)00074-3.

Sandi, S. G., J. F. Rodriguez, P. M. Saco, N. Saintilan, and G. Riccardi. 2021. "Accelerated Sea-Level Rise Limits Vegetation Capacity to Sequester Soil Carbon in Coastal Wetlands: A Study Case in Southeastern Australia." *Earth's Future* 9: e2020EF001901. https://doi.org/10.1029/2020EF001901.

Sapkota, Y., and J. R. White. 2021. "Long-Term Fate of Rapidly Eroding Carbon Stock Soil Profiles in Coastal Wetlands." *Science of the Total Environment* 753: 141913. https://doi.org/10.1016/j.scitotenv.2020.141913.

Shipley, B. 2013. "The AIC Model Selection Method Applied to Path Analytic Models Compared Using a D-Separation Test." *Ecology* 94: 560–564. https://doi.org/10.1890/12-0976.1.

Sinsabaugh, R. L. 2010. "Phenol Oxidase, Peroxidase and Organic Matter Dynamics of Soil." *Soil Biology and Biochemistry* 42: 391–404. https://doi.org/10.1016/j.soilbio.2009.10.014.

Sokol, N. W., and M. A. Bradford. 2019. "Microbial Formation of Stable Soil Carbon Is More Efficient From Belowground than Aboveground Input." *Nature Geoscience* 12: 46–53. https://doi.org/10.1038/s41561-018-0258-6.

Sun, M., M. Li, Y. Zhou, et al. 2023. "Nitrogen Deposition Enhances the Deterministic Process of the Prokaryotic Community and Increases the Complexity of the Microbial Co-Network in Coastal Wetlands." *Science of the Total Environment* 856: 158939. https://doi.org/10.1016/j.scitotenv.2022.158939.

Tang, B., K. S. Rocci, A. Lehmann, and M. C. Rillig. 2023. "Nitrogen Increases Soil Organic Carbon Accrual and Alters Its Functionality." *Global Change Biology* 29: 1971–1983. https://doi.org/10.1111/gcb.16588.

Tan, J., J. Huang, W. Quan, et al. 2025. "Divergence of Microbial Carbon Use Efficiency and Soil Organic Carbon Along a Tidal Flooding Gradient in A Subtropical Coastal Wetland." *Water Research* 280: 123527. https://doi.org/10.1016/j.watres.2025.123527.

Taillardat, P., B. S. Thompson, M. Garneau, et al. 2020. "Climate Change Mitigation Potential of Wetlands and the Cost-Effectiveness of Their Restoration." *Interface Focus*: 1020190129. https://doi.org/10.1098/rsfs.2019.0129.

Tong, C., J. Tan, M. Luo, et al. 2024. "Inundation Counteracts the Promoting Effect of Nitrogen Enrichment on Soil Organic Carbon Mineralization in a Tidal Marsh." *Fundamental Research*: S2667325824000360. https://doi.org/10.1016/j.fmre.2024.01.013.

Luo, M., Z. Zhai, R. Ye, R. Xing, J. Huang, and C. Tong. 2020. "Carbon Mineralization in Tidal Fresh Water Marsh Soils at the Intersection of Low-Level Saltwater Intrusion and Ferric Iron Loading." *Catena* 193: 104644. https://doi.org/10.1016/j.catena.2020.104644.

Wang, F., C. J. Sanders, I. R. Santos, et al. 2021*a*. "Global Blue Carbon Accumulation in Tidal Marshes Increases with Climate Change." *National Science Review* 8: nwaa296. https://doi.org/10.1093/nsr/nwaa296.

Wang, J., X. Shi, C. Zheng, H. Suter, and Z. Huang. 2021*b*. "Different Responses of Soil Bacterial and Fungal Communities to Nitrogen Deposition in a Subtropical Forest." *Science of the Total Environment* 755: 142449. https://doi.org/10.1016/j.scitotenv.2020.142449.

Whalen, E. D., A. S. Grandy, N. W. Sokol, et al. 2022. "Clarifying the Evidence for Microbial- and Plant-Derived Soil Organic Matter, and the Path Toward a More Quantitative Understanding." *Global Change Biology* 28: 7167–7185. https://doi.org/10.1111/gcb.16413.

Widdig, M., A. Heintz-Buschart, P. M. Schleuss, et al. 2020. "Effects of Nitrogen and Phosphorus Addition on Microbial Community Composition and Element Cycling in a Grassland Soil." *Soil Biology and Biochemistry* 151: 108041. https://doi.org/10.1016/j.soilbio.2020.108041.

Yu, G., Y. Jia, N. He, et al. 2019. "Stabilization of Atmospheric Nitrogen Deposition in China Over the Past Decade." *Nature Geoscience* 12: 424–429. https://doi.org/10.1038/s41561-019-0352-4.

Yu, G. H., and Y. Kuzyakov. 2021. "Fenton Chemistry and Reactive Oxygen Species in Soil: Abiotic Mechanisms of Biotic Processes, Controls and Consequences for Carbon and Nutrient Cycling." *Earth-Science Reviews* 214: 103525. https://doi.org/10.1016/j.earscirev.2021.103525.

Zang, H., I. Mehmood, Y. Kuzyakov, et al. 2024. "Not all Soil Carbon Is Created Equal: Labile and Stable Pools Under Nitrogen Input." *Global Change Biology* 30, no. 7: e17405. https://doi.org/10.1111/gcb.17405.

Zavarzina, A. G., T. A. Semenova, O. V. Belova, A. V. Lisov, A. A. Leontievskii, and A. E. Ivanova. 2018. "Laccase Production and Humic Acids Decomposition by Microscopic Soil Fungi." *Microbiology* 87: 308–316. https://doi.org/10.1134/S0026261718030153.

Supporting Information

Additional Supporting Information may be found in the online version of this article.

Submitted 11 December 2024
Revised 17 April 2025
Accepted 23 May 2025